Manuscript ID: DOEBTO-UMD-9158-24-TA1

Full Citation: Alam, T., Yang, J., Tancabel, J., Muehlbauer, J., & Hwang, Y., & Aute, V. (2024) **Optimization and Experimental Validation of Annular Finned PCM-HX for a Domestic Hot Water Heater Application.** *20th International Refrigeration and Air Conditioning Conference at Purdue*, July 15-18, 2024.

Optimization and Experimental Validation of Annular Finned PCM-HX for a Domestic Hot Water Heater Application

Tanjebul ALAM, Jangho YANG, James TANCABEL, Jan MUEHLBAUER, Yunho HWANG, Vikrant AUTE*

Center for Environmental Energy Engineering
Department of Mechanical Engineering, University of Maryland,
College Park, MD 20742, USA

*Corresponding Author: vikrant@umd.edu

ABSTRACT

The load profile for domestic water heating is time-dependent and can result in high energy demand during peak operating times. Shifting this peak load can have significant environmental and economic impacts. Phase change material (PCM)-based thermal energy storage (TES) is a potentially useful technology for peak load shifting in domestic hot water (DHW) applications thanks to its high latent heat and energy density. In this study, an annular finned-tube PCM-HX design concept was optimized for a load-shifting TES unit to meet the Department of Energy standard for a medium-usage DHW heater using a resistance-capacitance model (RCM) integrated with a Multi-Objective Genetic Algorithm. The optimized design comprised 70 identical annular finned-tube PCM-HX units connected in parallel and utilizing RT62HC as the PCM. A single PCM-HX unit was prototyped and tested in a vertically oriented setup with upward heat transfer fluid (HTF) flow. The hot water supply time was defined based on a cutoff temperature of 51.7°C. The as-designed mass flow rate (1.5 g/s) was tested to assess the performance of the prototyped PCM-HX unit for RCM validation.

For the experimental investigation, RTD sensor bundles measured HTF temperature at the PCM-HX inlet and outlet, and a Coriolis flow meter accurately measured the HTF mass flow rate. The simulated discharging power underpredicted the experimental result by about 12%, and the simulated hot water supply time underpredicted the experimental result by approximately 13% for the as-designed mass flow rate (1.5 g/s). The average deviation of the hot water supply temperature between the experimental and RCM results during the complete PCM solidification process was 1.3 K for the as-designed mass flow rate. The overall good agreement between the experimental and RCM results provides confidence that computationally efficient models such as RCM can be utilized for design optimization of PCM-HXs.

1. INTRODUCTION

With increasing residential energy demand worldwide and the pursuit of carbon emission reduction goals, there are global efforts towards the electrification of heating technologies combined with renewable energy sources. Regardless of power generation sources, overloading the electrical grid during peak hours can lead to operational issues in both power transmission and generation, as well as increased electricity costs for end-users (Blonsky et al., 2019). One potential solution to this challenge is shifting peak load demand to flatten energy demand spikes throughout the day. For thermal applications, Phase Change Material-based Thermal Energy Storage (PCM-TES) emerges as an excellent candidate to reduce and shift peak load demand by leveraging the latent heat of phase change transition of the material, enabling it to store and release larger amounts of energy compared to sensible energy storage systems.

Domestic hot water heating (DHW) systems stand as an ideal application for PCM due to their intermittent usage patterns, the need for temperature regulation, and the potential for load shifting. The literature presents several instances of PCM integration for domestic hot water heating (DHW) applications. Najafian et al. (2015) conducted a simulation study that integrated PCM modules into the hot water storage tank, optimizing PCM mass by varying parameters such as size (e.g., diameter, length), location, and number of PCM module containers to maximize hot water discharge time. Similarly, Nkwetta et al. (2014) and Kutlu et al. (2020) numerically investigated PCM modules placed inside the top section of the water storage tank, demonstrating the potential for peak load shifting and energy savings. In contrast, Jin et al. (2023) utilized PCM-TES located outside the water tank as a standalone component in the hot water supply system, conducting a numerical study on PCM-TES integrated with an air source heat pump unit to explore its potential for offsetting peak power demand and achieving financial savings. However, this study did not include experimental validation, and the heat transfer between the PCM and the working fluid took place at the external surfaces of the PCM volume. Amagour et al. (2018) experimentally investigated a compact tube-fin heat exchanger embedded in PCM to assess its performance for a DHW supply application and developed an ε-NTU relation. However, the heat exchanger configuration was not optimized.

This study considers component-level multi-objective optimization of liquid-to-PCM heat exchangers (PCM-HXs) targeting a U.S. Department of Energy (DOE)-standard medium-usage DHW heater (US Department of Energy, 2016) using a computationally efficient numerical PCM-HX solver. Comprehensive experimental testing was conducted using a conventionally-manufactured proof-of-concept optimal PCM-HX prototype to validate the RCM. Comparisons between the RCM and experimental results are provided to assess the accuracy of the RCM solver, particularly in predicting the hot water supply temperature from the PCM-HX, which is a crucial metric for evaluating the utility of the solver for this specific application.

2. METHODOLOGY

A resistance-capacitance based model (RCM) was developed for an annular finned-tube PCM-HX. Compared to past RCM work by the authors (Alam et al., 2022a,b), the present work includes conjugate heat transfer with a single-phase heat transfer fluid on the tube-side. The model was integrated with a multi-objective genetic algorithm (MOGA) (Deb, 2001) for optimization targeting a U.S. DOE standard medium-usage DHW application (US Department of Energy, 2016). Comprehensive experimental testing was conducted using a conventionally-manufactured proof-of-concept optimal PCM-HX prototype to validate the RCM. The overall approach is shown in Figure 1.

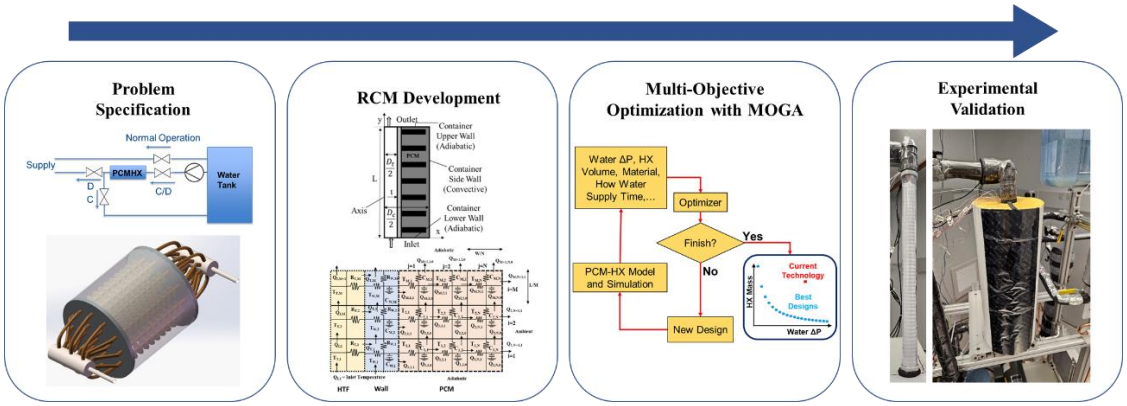

Figure 1: PCM-HX optimization approach.

3. PROBLEM DESCRIPTION

Storage-type water heaters have a tendency for tank water temperatures to drop below the set-point during daytime operation. This requires the water to be reheated above the set-point using (electrical) power input, which is undesirable during peak electricity consumption hours (Najafian et al., 2015). PCM-TES can be integrated into DHW heater systems to mitigate this issue. One such PCM-HX integration is illustrated in Figure 2-(L) (X. Yang et al., 2017). During peak periods (discharge (D) cycle in Figure 2-(L)), the PCM-HX heats the water before supply (PCM solidification), eliminating the need for heaters. The PCM-HX is charged (PCM melting) during off-peak hours using

heaters. In this work, we consider a PCM-HX with straight tubes and annular fins (Figure 2-(R)) which are connected in parallel while PCM occupies the remaining space in the tank.

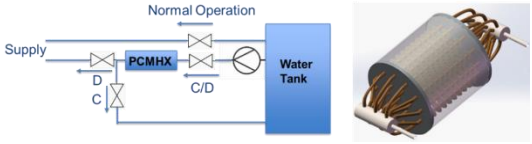

Figure 2: (Left) Operation diagram for PCM-HX integrated with domestic water heater system; (Right) Annular fin PCM-HX storage concept (X. Yang et al., 2017).

For effective heat extraction, the PCM must have a phase change temperature range sufficiently higher than the supply water temperature, which must meet or exceed 51.7°C as per the U.S. DOE standard (US Department of Energy, 2016). However, selecting a PCM with an excessively high phase-change temperature may complicate the recharge cycle by increasing recharge time and energy input. Accordingly, the organic PCM RT62HC (RUBITHERM GmbH) was chosen. The thermophysical properties of the PCM and the aluminum tube/fins are outlined in Table 1. Assuming that 25% of total daily hot water consumption will be supplied by the TES, the system must continuously deliver water at 51.7°C for at least 540 seconds at a flow rate of 6.4 L/min (US Department of Energy, 2016). The PCM-HX inlet water temperature was set to 46.7°C, considering a 5 K temperature drop during daytime operation due to heat loss. The initial temperature of the fully charged (melted) PCM-HX was assumed to be 65.7°C.

Table 1: Thermophysical properties of materials.

Material	**k (W/m-K)**	**ρ (kg/m^3)**	**c_p (J/kg-K)**	**T_{sol} - T_{melt} (°C)**	**ΔH (kJ/kg)**
RT62HC	0.2	850 (solid), 840 (liquid)	2000	60-64	230
Aluminum Alloy	170	2670	890	-	-

4. RCM DEVELOPMENT

RCMs are a lightweight alternative to computational fluid dynamics (CFD) for evaluating PCM-HX performance which simplifies the computational requirements by not solving for higher-order physics. Instead, RCMs rely on approximations of thermal resistance to achieve accurate results at a fraction of the computational cost typically associated with CFD simulations (Alam et al., 2022b). In this study, an RCM was developed for a cylindrical PCM-HX with straight tubes and annular fins, where PCM fills the annular space. The annular tube-fin geometry (Figure 3-(L)) involves conjugate heat transfer with a single-phase heat transfer fluid. Figure 3-(R) represents the RCM thermal network, which will be discussed in more detail in subsequent sections.

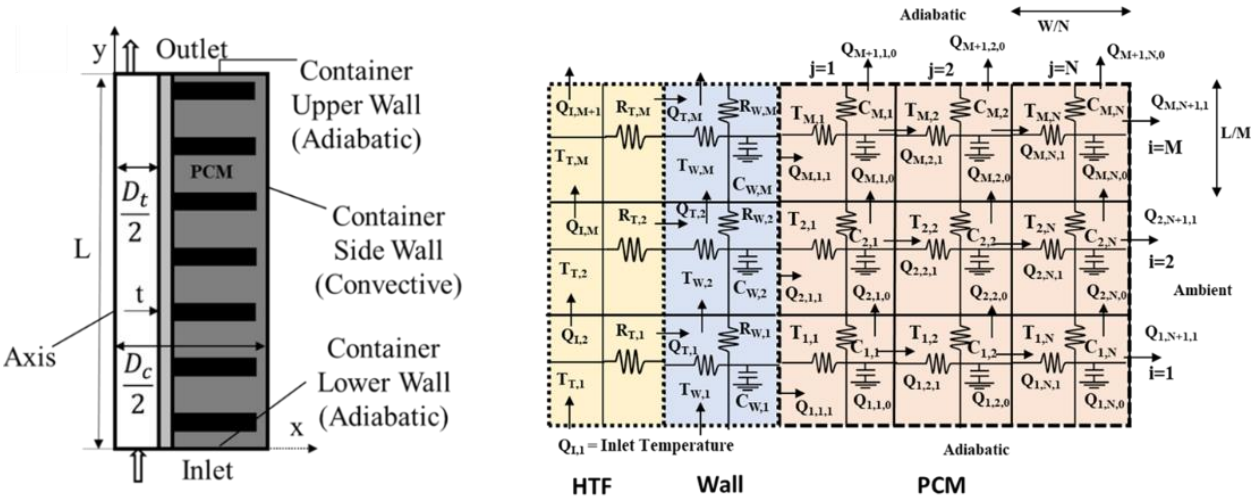

Figure 3: (Left) Computational domain of a cylindrical PCM-HX with a straight tube with annular fins; (Right) Thermal network of 2D RCM for annular finned PCM-HX.

4.1 RCM Assumptions

The general assumptions for the RCM are as follows. First, natural convection effects in the PCM are considered negligible, making the heat transfer conduction-dominated. Additionally, the properties of each segment are regarded as constant, and the entire segment can be described by a point at its center. Next, when both PCM and fins are present within a segment, they are treated as a composite medium, with effective material properties calculated based on the volumes of PCM and fin material within that segment, as outlined by Alam et al., (2022b). Moreover, the effect of contact resistance is ignored, ensuring a simplified calculation model. Additionally, no mass transfer occurs between segments, further simplifying the model and focusing purely on thermal properties. Finally, these assumptions help streamline the RCM for effective use in modeling and simulation.

4.2 RC Network Development

Figure 3-(R) depicts the thermal resistance-capacitance network for the annular tube-fin PCM-HX. The computational domain is segmented into three zones: (i) the heat transfer fluid (HTF) or "tube side", (ii) the tube wall, and (iii) the PCM / fins zone. As noted in Assumption 3, segments with both PCM and fins are treated as homogeneous segments with effective material properties determined based on the volumes of PCM/fin material present in that segment. The reader is referred to Alam et al. (2022b) for additional details on the non-uniform porosity calculation. The PCM and fin domains are discretized into equal-length segments in both the vertical and radial directions, while the tube and wall domains are discretized in the vertical direction only (i.e., one segment in the radial direction). Each segment has its own resistance and capacitance. Heat transfer between the tube and tube wall is calculated assuming laminar flow.

4.3 Explicit Time Marching Formulation

The time marching scheme is a first-order explicit Euler method to solve for the transient temperature profile in the PCM domain. The explicit time marching formulation for the annular finned PCM-HX is presented below.

The tube-side thermal network parameters are calculated using Equations (1)-(4):

$$R_{T,i,t} = \frac{1}{h_W A_T} \quad (1) \qquad \dot{Q}_{T,i,t} = \frac{T_{T,i,t} - T_{W,i,t}}{R_{T,i,t}} \quad (2)$$

$$T_{T,i,t} = T_{W,in};\ i = 1 \quad (3) \qquad T_{T,i,t} = T_{T,i-1,t} - \frac{\dot{Q}_{T,i,t}}{\dot{m}_W c_{p,W}};\ i \geq 2 \quad (4)$$

The wall thermal network parameters are calculated using Equations (5)-(10):

$$R_{W,i,R} = \frac{Mln\frac{D_o}{D_i}}{2\pi L k_W} \quad (5) \qquad \dot{Q}_{W,i+1,t} = \frac{T_{W,i,t} - T_{W,i+1,t}}{R_{W,i,V}} \quad (6)$$

$$\dot{Q}_{P,i,0,t} = \frac{T_{W,i,t} - T_{i,0,t}}{R_{W,i,t,R}} \quad (7) \qquad \frac{dT_{W,i,t+1}}{dt} = \frac{\dot{Q}_{T,i,t} + \dot{Q}_{W,i,t} - \dot{Q}_{W,i+1,t} - \dot{Q}_{P,i,0,t}}{C_{W,i,t}} \quad (8)$$

$$T_{W,i,t+\Delta t} = T_{W,i,t} + \frac{dT_{W,i,t}}{dt} \cdot \Delta t \quad (9) \qquad R_{W,i,V} = \frac{L\ /\ M}{k_W \cdot A_W} \quad (10)$$

The PCM/fin domain thermal network parameters are calculated using Equations **Error! Reference source not found.**-(18), and the RCM solver flowchart for the annular finned tube PCM-HX geometry is shown in Figure 4.

$$R_{P,i,j,R} = \begin{cases} \dfrac{Mln\ \frac{D_1}{D_0}}{2\pi L k_{eff}}; for\ i = 1 \\ \dfrac{Mln\ \frac{D_j}{D_{j-1}}}{2\pi L k_{eff}}; for\ i \geq 2 \end{cases} \quad (11) \qquad R_{P,i,j,V} = \frac{L/M}{k_{eff} \times A} \quad (12)$$

$$\dot{Q}_{i,j,t,0} = \begin{cases} 0 & ;for\ i = 1 \\ \dfrac{T_{i-1,j,t} - T_{i,j,t}}{R_{P,i,j,V}} & ;for\ i \geq 2 \end{cases} \quad (13)$$

$$\dot{Q}_{i,j,t,1} = \begin{cases} \dfrac{T_{i,j,t} - T_{i,j+1,t}}{R_{P,i,j,V}} & ;for\ i \geq 1 \\ \dfrac{T_{i,N,t} - T_{amb}}{R_{P,i,j,V}} & ;for\ i = N \end{cases} \quad (14)$$

$$\frac{dT_{i,j,t}}{dt} = \frac{\dot{Q}_{i,j,t,0} + \dot{Q}_{i,j,t,1} - \dot{Q}_{i+1,j,t,0} - \dot{Q}_{i,j+1,t,1}}{C_{i,j,t}} \quad (15)$$

$$T_{i,j,t+1} = T_{i,j,t} + \frac{dT_{i,j,t}}{dt} \times \Delta t \quad (16)$$

$$C_{PCM} = \begin{cases} C_s; & T < T_s \\ Cs + \dfrac{\Delta H}{T_{melt} - T_{sol}}; & T_s \leq T \leq T_l \\ C_l; & T > T_l \end{cases} \quad (17)$$

$$C_{i,j,t} = [\gamma\, C_{PCM}\, \rho_{PCM} + (1-\gamma)\, C_{FIN}\, \rho_{FIN}]\, V_{i,j} \quad (18)$$

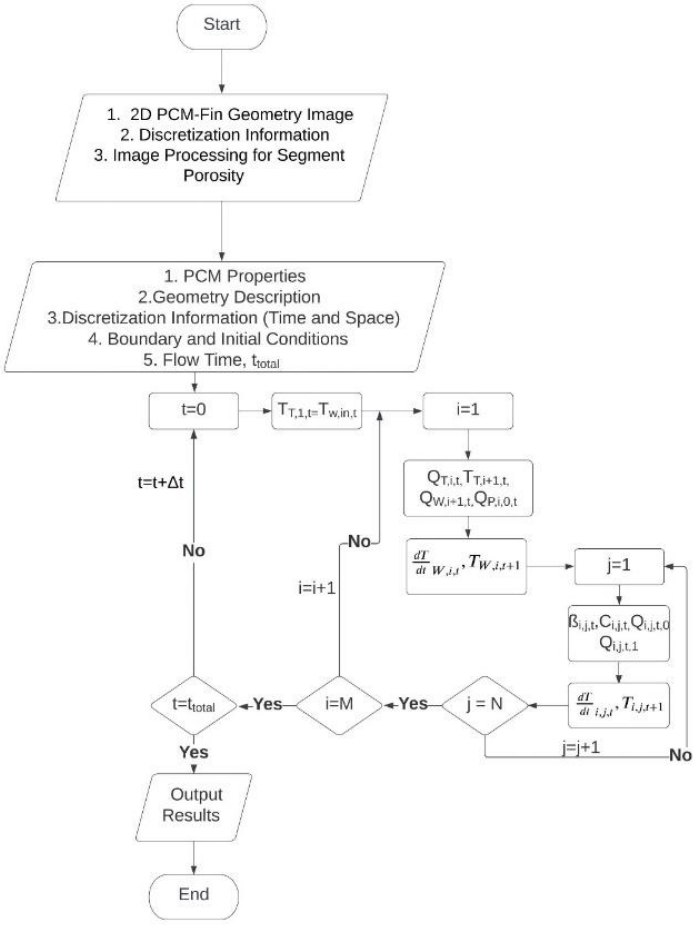

Figure 4: RCM solver flowchart for annular finned PCM-HX.

5. OPTIMIZATION AND DISCUSSION

5.1 Optimization Problem Formulation

The low computational cost of RCM makes it suitable for optimization using a multi-objective genetic algorithm (MOGA) (Deb, 2001). The overall objective is to design annular PCM-HXs to serve as a TES solution for mitigating heat loss from U.S. DOE standard medium-usage DHW heaters (US Department of Energy, 2016). The objective functions are to minimize the water pressure drop and minimize the total material mass (tube + fin mass) of PCM-HX (Equation (19)).

$$\min \Delta P_{Water}, M_{HX,Material} \quad (19)$$

$$s.t.$$
$$t_{HW} \geq 540s; \qquad V_{HX,total} \leq 0.1 \cdot V_{tank,baseline}; \quad -0.1 \leq SOC \leq 0.1$$

The baseline water heater tank volume was chosen based on a commercially-available electric water heater system. It was assumed that there is no heat loss to ambient. The design space is detailed in **Table 2**, where tube diameter, fin thickness, and container diameters are discrete variables based on the availability of off-the-shelf aluminum tubes, aluminum fins, and polycarbonate tubes. Additionally, two tube thicknesses were chosen. The continuous variables, fin pitch and tube length, are chosen based on previous experience with annular-fin PCM-HXs, and the number of parallel units is chosen to ensure the PCM-HX achieves the required capacity.

Table 2: Optimization design space.

Continuous Variables	**Lower Limit**	**Upper Limit**
Fin Pitch (mm), F_P	0.2 D_f	0.5D_f
Length (mm), L	300	700
Discrete Variables	**Values**	
Outer Tube Diameter (mm), D_t	15.87, 12.7, 9.52, 7.94 6.35,4.76 (t_t =0.89) 9.52, 6.35 (t_t =0.71)	
Fin Thickness (mm), t_f	0.81,0.63,0.41,0.25	
Container Diameter (mm), D_C	25.4, 28.58, 31.75, 34.93, 38.1, 44.45, 50.8, 57.15,63.5	
Number of Parallel Units, N	20-82	

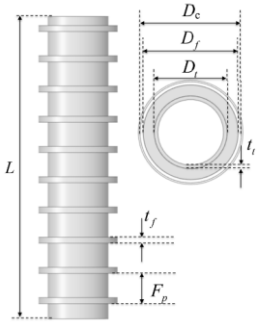

The optimization constraints include the total hot water supply time, the total HX volume, and the State of Charge (SOC). The minimum total hot water supply time is predetermined as 540 seconds (US Department of Energy, 2016). The thermal energy storage (TES) volume was constrained to 10% of the original system volume (254,600 cm³), in accordance with the U.S. DOE target for TES systems (US Department of Energy, 2016).
The final constraint is based on the State of Charge defined as the ratio of energy stored in the TES at a specific time to the theoretical maximum energy storage, and ensures that the TES primarily remains in the latent region during PCM-HX operation (Equation (20)).

$$SOC(t) = \frac{Remaining\ energy\ stored\ (t)}{Theoretical\ maximum\ storeable\ energy} \tag{20}$$

5.2 Optimization Results and Discussion

The annular tube-fin PCM-HX optimization results are shown in Figure 5. The color scale indicates the PCM-HX discharge time, i.e., the total time the PCM-HX can supply hot water before the outlet temperature falls below the set-point temperature. The marker size corresponds to the total PCM-HX volume. Six optimal designs are further analyzed, each representing a cluster of designs with similar characteristics (e.g., geometry and performance).

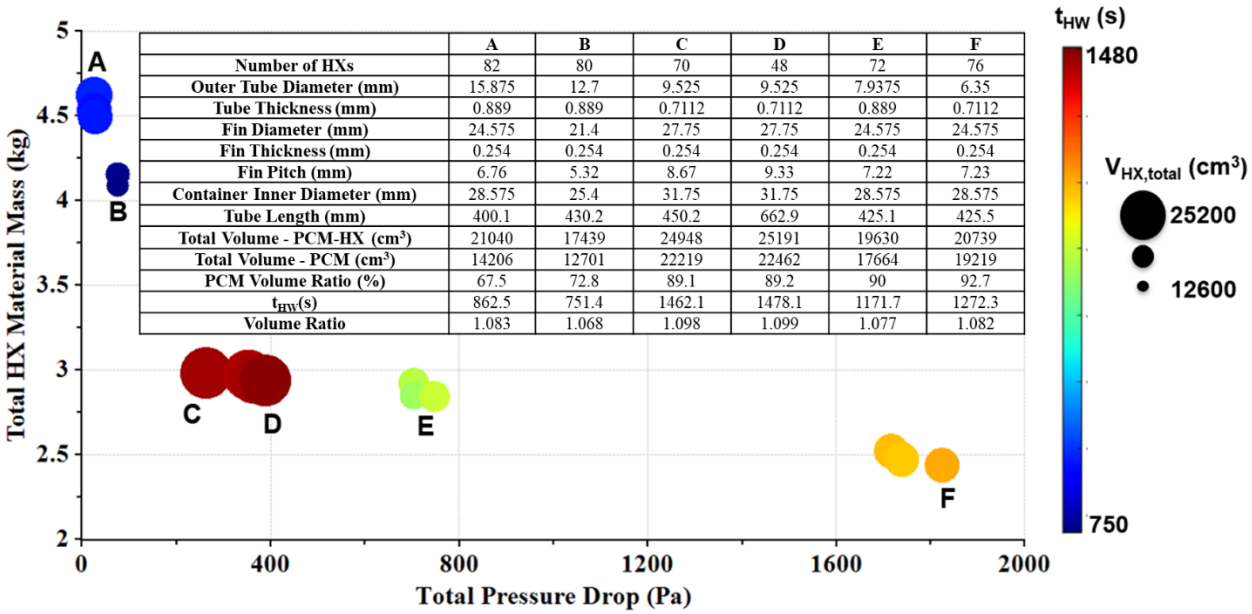

	A	B	C	D	E	F
Number of HXs	82	80	70	48	72	76
Outer Tube Diameter (mm)	15.875	12.7	9.525	9.525	7.9375	6.35
Tube Thickness (mm)	0.889	0.889	0.7112	0.7112	0.889	0.7112
Fin Diameter (mm)	24.575	21.4	27.75	27.75	24.575	24.575
Fin Thickness (mm)	0.254	0.254	0.254	0.254	0.254	0.254
Fin Pitch (mm)	6.76	5.32	8.67	9.33	7.22	7.23
Container Inner Diameter (mm)	28.575	25.4	31.75	31.75	28.575	28.575
Tube Length (mm)	400.1	430.2	450.2	662.9	425.1	425.5
Total Volume - PCM-HX (cm³)	21040	17439	24948	25191	19630	20739
Total Volume - PCM (cm³)	14206	12701	22219	22462	17664	19219
PCM Volume Ratio (%)	67.5	72.8	89.1	89.2	90	92.7
t_{HW}(s)	862.5	751.4	1462.1	1478.1	1171.7	1272.3
Volume Ratio	1.083	1.068	1.098	1.099	1.077	1.082

Figure 5: Annular finned PCM-HX optimization results with a tabulated summary of six selected designs.

Moving from left to right in Figure 5, the tube diameters and the number of parallel units generally decrease, leading to a greater water pressure drop. Larger tube diameters, lower fin pitches, and a higher number of parallel units contribute to the higher PCM-HX mass. Despite similarities in most aspects, designs C and D differ notably in tube length and the number of parallel units. Design D compensates for a lower number of parallel units with a tube length that is ~50% longer than the other designs.

6. EXPERIMENTAL VALIDATION

A single PCM-HX unit was fabricated and tested using a PCM-to-HTF test facility (Yang et al. (2022)) to experimentally validate the RCM and optimization results. The reader is referred to Yang et al. (2022) for additional details on the test facility.

6.1 PCM-HX Prototype Description

Design C (Figure 5) was selected for fabrication due to its balance between total HX mass, overall pressure drop, and notably, the predicted hot water supply time (1462 seconds), which is 2.71 times longer than the minimum required supply time (540 seconds). Table 3 provides an overview of the fabricated PCM-HX. Slight adjustments were made to Design C, notably the container and tube lengths, to prevent PCM leakage resulting from PCM volume expansion during the melting process. Moreover, an Al-3003 tube with a slightly smaller inner diameter was utilized since the as-designed Al-6061 tube resulted in incomplete brazing between the tubes and fins. In total, 272.6 g of RT62HC was added to the PCM-HX container, resulting in an 89% PCM-to-container volume ratio.

Table 3: Single PCM-HX Unit Configuration

Container Length [mm]	475.2	Fin Pitch [mm]	8.67
Container Diameter [mm]	31.75 [ID], 38.1 [OD]	Number of Fins	52
HX Tube Diameter [mm]	7.75 [ID], 9.53 [OD]	PCM Mass [g]	272.6
Fin Diameter [mm]	27.75	Charged Liquid PCM level [mm]	460.2
Fin Thickness [mm]	0.25	PCM Volume to Container Inner Volume Ratio [%]	89

Figure 6-(L) depicts the positions of the installed thermocouple. All temperature sensors were calibrated with highly accurate reference RTDs and a thermal bath. In total, 17 thermocouples were installed in and around the PCM-HX. On the PCM side, three thermocouples were installed between the HX fins using the 3D-printed holders. Ten

thermocouples were installed on the outer surface of the container, and two pairs of two thermocouples were installed on the inner and outer sides of the container top and bottom covers. Water-side temperature measurements were recorded using two sets of three RTDs. Figure 6-(R) displays the complete setup with the PCM-HX insulated with three inches of R-13 fiberglass insulation to minimize heat loss through the container to the ambient.

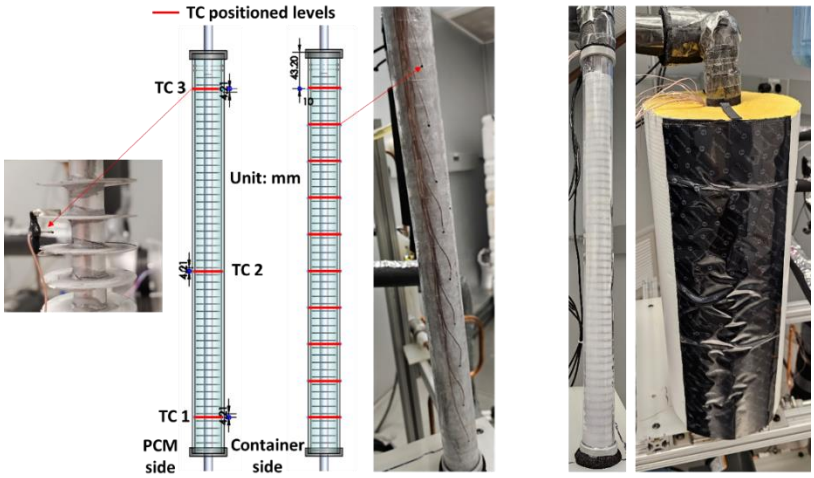

Figure 6: (Left) Installed thermocouple positions; (Right) Completed test setup with PCM and fiberglass insulation.

6.2 PCM-HX Test Results

As described in Section 3, the as-designed total water volume flow rate of 6.4 L/min was selected. For a single PCM-HX unit of Design C, this is equivalent to a mass flow rate of ~1.5 g/s. The PCM-HX water flow direction was upward. Three repeatability tests were performed, and the temperature reading differences were negligible; thus, the detailed results are omitted for brevity. It is noteworthy that the tube-side pressure drop was not experimentally measured, as the primary focus during RCM validation was to assess the heat transfer characteristics of the PCM-HX. The comparison of as-designed simulated and experimental PCM-HX performance is summarized in **Table 4**.

	Hot Water Supply Time	Discharge Power until Cutoff T
Experimental PCM-HX	23.5 min	45.5 W (±0.4% average uncertainty)
Simulated (as-designed) PCM-HX (Percent error w.r.t. experiment)	20.3 min (-13.6%)	39.9 W (-12.3%)

	Hot Water Supply Time	Discharge Power until Cutoff T
Experimental PCM-HX	23.5 min	45.5 W (±0.4% average uncertainty)
Simulated (as-designed) PCM-HX (Percent error w.r.t. experiment)	20.3 min (-13.6%)	39.9 W (-12.3%)

Table 4: Test condition and results with 1.5 g/s mass flow rate.

In **Table 4**, the "hot water supply time" indicates the total time until the outlet water temperature reaches the cutoff temperature (51.7°C); the average inlet water temperature was ~46.7°C. Meanwhile, "discharge power" indicates the heat transfer rate during the hot water supply period as the pre-melted PCM solidifies. While the original simulation results indicated a hot water supply time of 24.4 minutes, the supply time reported here is 20.3 minutes. Ultimately, the RCM underpredicted the experimental hot water supply time and discharge power by 13.6% and 12.3%, respectively. These discrepancies are attributed to multiple items, i.e., minor design modifications during prototyping (see Section 6.1), the as-designed PCM-HX assuming a constant inlet water temperature while the experimental inlet

temperature was not constant, and additional thermal masses introduced by the container, container covers, and insulation. Another potential source of uncertainty may include the assumption of a uniform, constant PCM-HX initial temperature; i.e., the PCM-HX initial temperature is determined as the average of the three internal thermocouples, while the actual PCM-HX temperature is likely vertically-stratified rather than uniformly distributed.

The predicted and experimental hot water supply temperatures are plotted along with the reference cutoff temperature (51.7°C) in Figure 7. It was observed that the maximum deviation occurred at the beginning of the test when the temperatures were rapidly changing. During the remainder of the test, the temperature deviation remained below 2 K, with an average deviation of 1.3 K over the entire PCM discharging process, indicating a strong agreement between the experimental and RCM results.

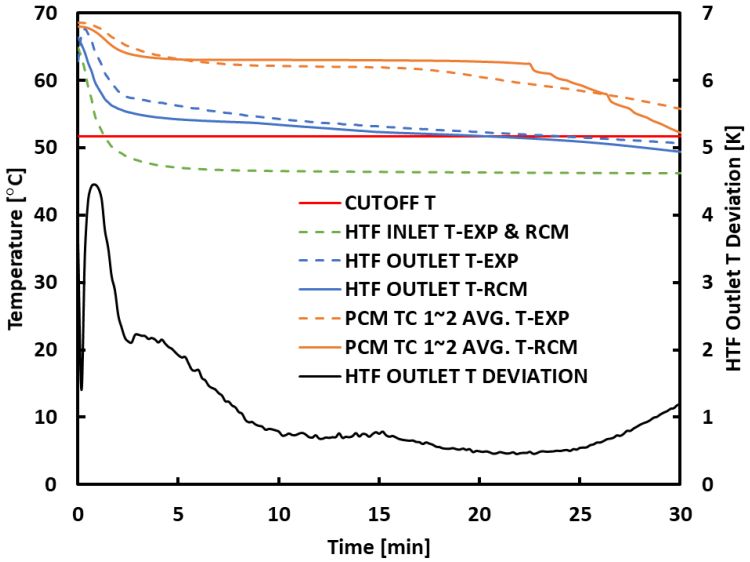

Figure 7: Comparison between experimental and RCM results during hot water drawing test (PCM solidification).

The HTF inlet temperature profile and the PCM average temperature from Thermocouples 1 and 2 are also plotted in Figure 7 for reference. Note that Thermocouple 3 (located near the top of the PCM-HX) was excluded as it became exposed to the air during PCM solidification, and thus cannot provide useful test data. The trends observed in both the experimental and simulation data for the average PCM temperature and hot water supply time were closely aligned. It is important to highlight that the hot water supply time, a critical metric in this context, consistently showed great agreement between the experimental and RCM results.

7. CONCLUSION

In this study, a computationally-efficient resistance-capacitance model (RCM) was developed for annular tube-fin PCM-HXs and integrated with a MOGA to design PCM-HXs for a U.S. DOE standard medium draw DHW application. A single unit of an optimal PCM-HX design was fabricated and tested to experimentally validate the RCM and optimization framework. Overall, a good agreement was found between the simulated and experimental performance. The average hot water supply temperature deviation throughout the solidification process was ~1.3 K, while the errors for total hot water supply time and discharge power were 13% and 12%, respectively. This provides confidence in the capability of RCM coupled with MOGA to design-optimize annular tube-fin PCM-HXs more efficiently and with similar accuracy to high-computational-cost CFD-based methods.

NOMENCLATURE

A	segment area	(m^2)	**Subscripts**	
C	heat capacity, thermal capacitance	(kJ/kg-K)	*amb*	ambient

c_p	specific heat	(kJ/kg-K)	C	container
D	diameter	(mm)	*eff*	effective
F_p	fin pitch	(mm)	*f*	fins
h	heat transfer coefficient	(W/m^2-K)	*HX*	heat exchanger
ΔH	latent heat	(kJ/kg)	*HW*	hot water
k	thermal conductivity	(W/m-K)	*i*	segment number (vertical)
L	length, height of the computational domain	(m)	*in*	inlet
$\dot{m}$	mass flow rate	(kg/s)	*j*	segment number (radial)
M	mass	(kg)	*l*	liquid
ΔP	pressure drop	(Pa)	*melt*	melting
$\dot{Q}$	heat flow	(W)	*P*	PCM
R	thermal resistance	(K/W)	*R*	radial direction
SOC	state of charge	(%)	*s*	solid
t	thickness, time	(mm), (s)	*sol*	solidification
Δt	time step	(s)	*t*	tube
T	temperature	(°C)	*W*	tube wall
V	volume	(cm^3)	*0*	vertical heat flow
W	radial dimension of the computational domain	(m)	*1*	radial heat flow
β	liquid fraction	(-)		
γ	PCM porosity	(-)		
ρ	density	(kg/m^3)		

REFERENCES

Alam, T., Bacellar, D., Ling, J., & Aute, V. (2022). Development and Validation of Resistance-Capacitance Model for Phase Change Material Embedded in Porous Media. *2022 21st IEEE Intersociety Conference on Thermal and Thermomechanical Phenomena in Electronic Systems (iTherm)*, 1–7. https://doi.org/10.1109/iTherm54085.2022.9899532

Alam, T., Righetti, G., Bacellar, D., Aute, V., & Mancin, S. (2022). Development and Validation Of Resistance-Capacitance Model (RCM) For Phase Change Material (PCM) Embedded In 3D Periodic Structures. *International Refrigeration and Air Conditioning Conference. Paper 2300.* https://docs.lib.purdue.edu/iracc/2300

Amagour, M. E. H., Rachek, A., Bennajah, M., & Ebn Touhami, M. (2018). Experimental investigation and comparative performance analysis of a compact finned-tube heat exchanger uniformly filled with a phase change material for thermal energy storage. *Energy Conversion and Management*, *165*(December 2017), 137–151. https://doi.org/10.1016/j.enconman.2018.03.041

Blonsky, M., Nagarajan, A., Ghosh, S., McKenna, K., Veda, S., & Kroposki, B. (2019). Potential Impacts of Transportation and Building Electrification on the Grid: A Review of Electrification Projections and Their Effects on Grid Infrastructure, Operation, and Planning. *Current Sustainable/Renewable Energy Reports*, *6*(4), 169–176. https://doi.org/10.1007/s40518-019-00140-5

Deb, K. (2001). *Multiobjective Optimization Using Evolutionary Algorithms. Wiley, New York*.

Jin, X., Zheng, S., Huang, G., & CK Lai, A. (2023). Energy and economic performance of the heat pump integrated with latent heat thermal energy storage for peak demand shifting. *Applied Thermal Engineering*, *218*, 119337. https://doi.org/10.1016/j.applthermaleng.2022.119337

Kutlu, C., Zhang, Y., Elmer, T., Su, Y., & Riffat, S. (2020). A simulation study on performance improvement of solar assisted heat pump hot water system by novel controllable crystallization of supercooled PCMs. *Renewable Energy*, *152*, 601–612. https://doi.org/10.1016/j.renene.2020.01.090

Najafian, A., Haghighat, F., & Moreau, A. (2015). Integration of PCM in domestic hot water tanks: Optimization for shifting peak demand. *Energy and Buildings*, *106*, 59–64. https://doi.org/10.1016/j.enbuild.2015.05.036

Nkwetta, D. N., Vouillamoz, P.-E., Haghighat, F., El Mankibi, M., Moreau, A., & Desai, K. (2014). Phase change materials in hot water tank for shifting peak power demand. *Solar Energy*, *107*, 628–635. https://doi.org/10.1016/j.solener.2014.05.034

RUBITHERM GmbH. (n.d.). *RT62HC*. https://www.rubitherm.eu/media/products/datasheets/Techdata_-RT62HC_EN_09102020.PDF

US Department of Energy. (2016). *Code of Federal Regulations, 2016, Title 10 – Energy, Chapter X - DEPARTMENT OF ENERGY (GENERAL PROVISIONS)*.

Yang, J., Muehlbauer, J., Bacellar, D., Ling, J., Aute, V., & Hwang, Y. (2022). *Experimental Investigation of a Phase Change Material Charged Finned-Tube Heat Exchanger*.

Yang, X., Lu, Z., Bai, Q., Zhang, Q., Jin, L., & Yan, J. (2017). *Thermal performance of a shell-and-tube latent heat thermal energy storage unit: Role of annular fins*. *202*, 558–570. https://doi.org/10.1016/j.apenergy.2017.05.007

ACKNOWLEDGEMENT

This material is based upon work supported by the U.S. Department of Energy's Office of Energy Efficiency and Renewable Energy (EERE) under the Building Technologies Office (BTO) Award Number DE-EE0009158. The views expressed herein do not necessarily represent the views of the U.S. Department of Energy or the United States Government. This work was also supported in part by the Modeling & Optimization Consortium and Energy Efficiency & Heat Pumps Consortium at the Center for Environmental Energy Engineering at the University of Maryland. The authors would like to acknowledge Y. Shabtay and J. Black of Heat Transfer Technologies, LLC, for their manufacturing expertise which contributed to the production of the HX prototype studied in this work.